A.B. El-Bediwi et al. (2016) Int J Appl Sci Biotechnol, Vol 4(3): 417-424
DOI: 10.3126/ijasbt.v4i3.15781

ISSN (Online): 2091-2609
DOI Prefix: 10.3126/ijasbt
International Journal of Applied Sciences and Biotechnology
(IJASBT)

Research Article

# INFLUENCE OF TITANIUM DIOXIDE NANOPARTICLES ON MICROSTRUCTURE, ELECTROCHEMICAL CORROSION BEHAVIOR, MECHANICAL AND THERMAL PROPERTIES OF Sn-Al-Bi BASED ALLOY

**Abu Bakr El-Bediwi[1*], N.A. El-Shishtawi[1] and Manal Mawloud Abdullah[1, 2]**

[1]Metal Physics Lab., Physics Department, Faculty of Science, Mansoura University, Egypt
[1, 2]Faculty of Education Aboaesa, University of Alzawya, Libya

*Corresponding author's email: baker_elbediwi@yahoo.com

## Abstract

Effect of adding titanium dioxide nanoparticles on microstructure, Vickers hardness, internal friction, thermal parameters and electrochemical corrosion behavior of $Sn_{76}Al_{10}Bi_{10}Cu_2Zn_2$ alloy has been studied using different experimental techniques. Crystallinity (peak intensity), crystal size (peak broadness) and orientations (peak position, 2θ) of $Sn_{76}Al_{10}Bi_{10}Cu_2Zn_2$ alloy changed after adding titanium dioxide nanoparticles. Corrosion resistance and internal friction of $Sn_{76}Al_{10}Bi_{10}Cu_2Zn_2$ alloy improved after adding titanium dioxide nanoparticles. Vickers hardness value of $Sn_{76}Al_{10}Bi_{10}Cu_2Zn_2$ alloy varied decreased after adding titanium dioxide nanoparticles.

**Keywords:** corrosion parameters; Vickers hardness; internal friction; titanium dioxide nanoparticles

## Introduction

Tin- aluminum alloys have good mechanical properties with conformability but these are quite costly. Aluminum-tin alloys have been used as bearing materials (Forrester PG, 1960) which carry a good combination of strength and surface properties (Pratt GC, 1973). Aluminum- tin based alloys are widely used as sliding bearing materials in automobile and shipbuilding industry (Desaki *et al.*, 2000, Lepper *et al.*, 1997). Tin phase in Al-Sn bearing materials can provide suitable friction properties and shear surface during sliding because it's low modulus, low strength and the excellent anti-welding characteristics with iron (Desaki *et al.*, 2000). Aluminum- tin and lead- aluminum alloys slightly differ in mechanical properties (Pathak and Mohan, 2003). Indium and lead have lowest elastic modulus of all the soft phases alloying with aluminum (Tegart, 1966). The fatigue strength of cold worked and heat treated $AlSn_{20}Cu_1$ alloy having reticular structure is close to that of $CuPb_{30}$ alloy with higher seizure resistance (Forrester, 1961). Strength and ductility of $SnSb_5$ alloy improved after adding Bi or Cu content (Esfandyarpour and Mahmudi, 2011). Elastic modulus and internal friction of $Sn_{86}Sb_{10}Cu_2X_2$ (X = Pb or Ag or Se or Cd- Zn) alloys dependent on alloy composition (El-Bediwi *et al.*, 2011). Effect of adding Cu or Ag or CuAg on structure, electrical resistivity and elastic modulus of $SnSb_7$ alloy has been studied and the results show, $SnSb_7Ag_2Cu_2$ alloy has lowest internal friction, cast and adequate elastic modulus (El-Bediwi, 2004). Adding 1 wt. % Cu or Ag improved mechanical properties of SnSb alloy (El-Bediwi, 2004). Both ultimate tensile strength and ductility of $SnSb_5$ alloy increased after adding Bi or Cu (Esfandyarpour and Mahmudi, 2011). Elastic modulus, internal friction, hardness and thermal conductivity of Sn-Sb alloy improved after adding (CuPb) elements (Kamal, 2006). Elastic modulus, Vickers hardness and thermal diffusivity of $Sn_{87}Sb_{10}Pb_3$ and $Sn_{80}Al_{20}$ alloys increased after adding $TiO_2$ nanoparticles. Internal friction, thermal conductivity and specific heat of $Sn_{87}Sb_{10}Pb_3$ and $Sn_{80}Al_{20}$ alloys varied after adding $TiO_2$ nanoparticles. Adding titanium oxide nanoparticles improved strengthens and internal friction of $Sn_{87}Sb_{10}Pb_3$ and $Sn_{80}Al_{20}$ alloys (El-Bediwi, 2015). Strengths of tin- antimony- lead and tin- aluminum- antimony- lead alloys increased after adding titanium oxide. Also stress exponent of tin- antimony- lead and tin- aluminum- antimony- lead alloys decreased after adding titanium oxide (El- Bediwi, 2015). Corrosion parameters, elastic modulus, internal friction, Vickers hardness, electrical resistivity and thermal parameters of $SnSb_{13}$ alloy varied after adding Cu, Bi, Al, Zn and Ag element (El- Bediwi, 2015). Melting point, mechanical properties, contact angle and electrochemical parameters of $Sn_{72}Zn_4Bi_{24}$ alloy varied after adding Cu, In, Al, Se and Ag contents. Adding Cu, Al, Se and Ag content improve mechanical and electrical properties of $Sn_{72}Zn_4Bi_{24}$ alloy (El- Bediwi, 2015). The aim of this work was to study the effect of titanium dioxide on microstructure, electrochemical corrosion behavior, thermal process, internal friction and Vickers hardness of $Sn_{76}Al_{10}Bi_{10}Cu_2Zn_2$ alloy.

## Experimental Work

$Sn_{76}Al_{10}Bi_{10-x}Cu_2Zn_2(TiO_2)_x$ alloys were prepared using tin, aluminum, bismuth, zinc, copper and titanium dioxide with purity better than 99.5 %. The $Sn_{76}Al_{10}Bi_{10-x}Cu_2Zn_2(TiO_2)_x$ alloys melted in a muffle furnace and the resulting ingots were turned and re-melted again to increase the homogeneity. From these alloys long ribbons of ~ 4 mm width and ~ 90 µm thicknesses were prepared by single roller melt spinning technique. Using double knife cuter the samples cut into convenient shape for all measurements. Microstructure of used alloys was performed using Shimadzu X–ray Diffractometer, (Dx–30, Japan) Cu–Kα radiation with λ=1.54056 Å at 45 kV and 35 mA and Ni–filter, in the angular range 2θ ranging from 0 to 100° in continuous mode with a scan speed 5 deg/min and scanning electron microscope (JEOL JSM-6510LV, Japan). The polarization studies were performed using Gamry Potentiostat/Galvanostat with a Gamry framework system based on ESA 300. Gamry applications include software DC105 for corrosion measurements, and Echem Analyst version 5.5 software packages for data fitting. The differential scanning calorimetry (DSC) thermographs were obtained by SDT [Q600 (V20.9 Build 20), U. S. A] instrument with heating rate 10 k/min in the temperature range 0-400 °C. A digital Vickers micro-hardness tester, (Model-FM-7- Japan), was used to measure Vickers hardness values. The internal friction $Q^{-1}$ was determined using the dynamic resonance method (Cullity, 1959, Schreiber *et al.*, 1973, Timoshenko and Goddier 1951) by plotting the amplitude of vibration against the frequency of vibration. The thermal diffusivity $D_{th}$ has been derived from resonance peak (Berry and Pritchett, 1973).

***Microstructure***

***X-Ray Analysis***

Fig. 1 (a, b, c and d) shows x-ray diffraction patterns of $Sn_{76}Al_{10}Bi_{10-x}Cu_2Zn_2(TiO_2)_x$ alloys. Fig. 1a shows the $Sn_{76}Al_{10}Bi_{10}Cu_2Zn_2$ alloy has sharp lines corresponding to β-Sn phase and hexagonal Bi phase with started base line ~ 100 counts. $Sn_{76}Al_{10}Bi_{10-x}Cu_2Zn_2(TiO_2)_x$ alloys have sharp lines corresponding to tetragonal β-Sn phase and hexagonal Bi phase with various started base line (increased started base line up to 1 wt.% $TiO_2$ nanoparticle and then decreased). Also crystallinity (peak intensity), crystal size (peak broadness) and orientations (peak position, 2θ) of $Sn_{76}Al_{10}Bi_{10}Cu_2Zn_2$ alloy changed after adding titanium dioxide nanoparticles as shown in Fig. 1(a- d). The detail of x-ray analysis of $Sn_{76}Al_{10}Bi_{10-x}Cu_2Zn_2(TiO_2)_x$ alloys from the x-ray device (2θ, Int. %, d Å, FHWM and area) and from x-ray cards (phase and Miller indices) are listed in Table 1 (a, b, and c)**.** The analysis show that, Al, Cu, Zn atoms and $TiO_2$ nanoparticle dissolved in matrix formed a solid solution and\or undetected phases and changed its microstructure. The estimated crystal size was given through measured diffraction pattern broadening by Scherer formula (Cullity, 1959). Crystal size of β- Sn phase in $Sn_{76}Al_{10}Bi_{10}Cu_2Zn_2$ alloy varied increased after adding titanium dioxide as presented in Table 1d. Lattice microstain of $Sn_{76}Al_{10}Bi_{10-x}Cu_2Zn_2(TiO_2)_x$ alloys were calculated from the relation between full half width maximum (FHWM) and 4tanθ as shown in Fig. 1e. Lattice microstrain of $Sn_{76}Al_{10}Bi_{10}Cu_2Zn_2$ alloy decreased after adding titanium dioxide up to 1 wt. % and then increased as listed in Table 1e. The $Sn_{76}Al_{10}Bi_9Cu_2Zn_2(TiO_2)_1$ alloy has lower microstrain value.

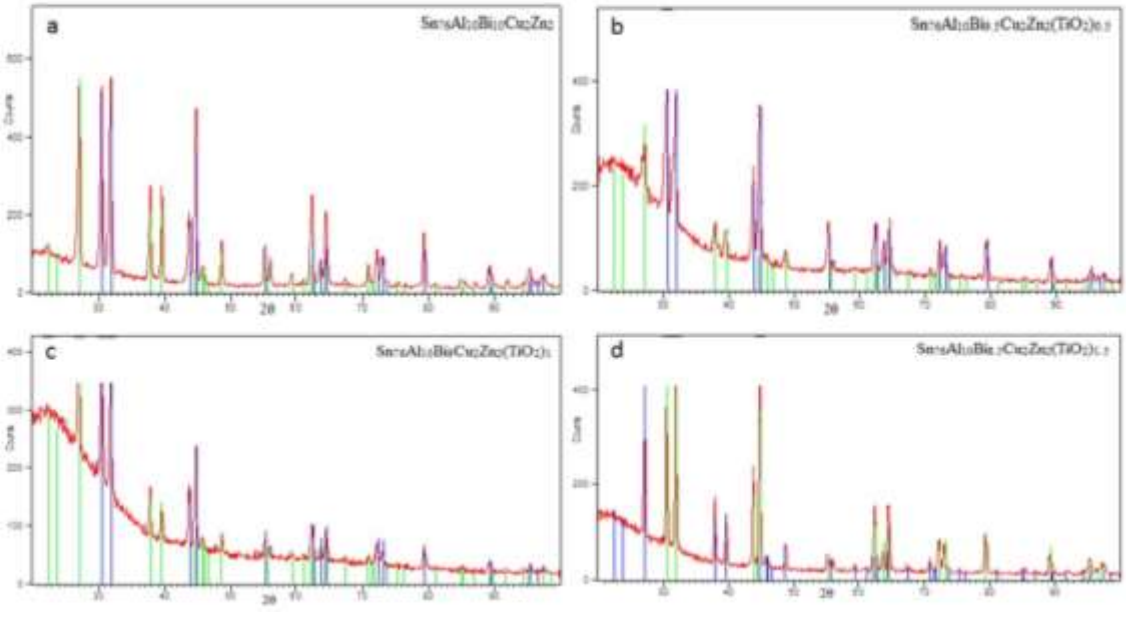


**Fig. 1:** x-ray diffraction patterns of $Sn_{76}Al_{10}Bi_{10-x}Cu_2Zn_2(TiO_2)_x$ alloys (**a**. $Sn_{76}Al_{10}Bi_{10}Cu_2Zn_2$ alloy; **b**: $Sn_{76}Al_{10}Bi_{9.5}Cu_2Zn_2(TiO_2)_{0.5}$ alloy; **c**: $Sn_{76}Al_{10}Bi_9Cu_2Zn_2(TiO_2)_1$ alloy; **d**: $Sn_{76}Al_{10}Bi_{8.5}Cu_2Zn_2(TiO_2)_{1.5}$ alloy)

**Table 1a**: x-ray analysis of $Sn_{76}Al_{10}Bi_{9.5}Cu_2Zn_2(TiO_2)_{0.5}$ alloy

| 2θ | d Å | Int. % | FHWM | Area | Phase | hkl |
|---|---|---|---|---|---|---|
| 22.4786 | 3.95541 | 27.53 | 0.6512 | 46.8 | Bi | 003 |
| 27.1518 | 3.28431 | 28.08 | 0.2362 | 25.61 | Bi | 012 |
| 30.5839 | 2.92312 | 100 | 0.2558 | 98.81 | Sn | 200 |
| 31.9781 | 2.79879 | 60.98 | 0.1968 | 46.35 | Sn | 101 |
| 37.8853 | 2.37488 | 15.72 | 0.3936 | 23.9 | Bi | 104 |
| 39.6099 | 2.27536 | 12.39 | 0.4723 | 22.61 | Bi | 110 |
| 43.7345 | 2.06987 | 45.89 | 0.2165 | 38.37 | Sn | 220 |
| 44.8222 | 2.02213 | 74.02 | 0.1968 | 56.26 | Bi | 110 |
| 45.93 | 1.97591 | 2.55 | 0.09 | 0.9 | Sn | 220 |
| 48.7059 | 1.86959 | 8.2 | 0.3149 | 9.98 | Bi | 110 |
| 55.2163 | 1.66357 | 23.7 | 0.1968 | 18.02 | Sn | 310 |
| 59.15 | 1.56198 | 2.3 | 0.09 | 0.81 | Bi | 107 |
| 62.4016 | 1.48818 | 23.75 | 0.3149 | 28.89 | Bi | 107 |
| 63.6835 | 1.46128 | 14.57 | 0.2755 | 15.51 | Bi | 107 |
| 64.456 | 1.44562 | 26.82 | 0.2952 | 30.57 | Sn | 321 |
| 70.8339 | 1.3303 | 3.44 | 0.4723 | 6.28 | Bi | 214 |
| 72.2323 | 1.30795 | 17.73 | 0.3149 | 21.56 | Sn | 420 |
| 73.0462 | 1.29537 | 14.13 | 0.3149 | 17.18 | Sn | 411 |
| 79.3003 | 1.20818 | 18.41 | 0.1968 | 13.99 | Sn | 312 |
| 89.1482 | 1.09847 | 10.29 | 0.4723 | 18.78 | Sn | 501 |
| 95.4695 | 1.04175 | 5.55 | 0.6298 | 13.49 | Sn | 332 |
| 97.2988 | 1.02613 | 3.87 | 0.576 | 11.63 | Sn | 521 |

**Table 1b**: x-ray analysis of $Sn_{76}Al_{10}Bi_9Cu_2Zn_2(TiO_2)_1$ alloy

| **2θ** | **d Å** | **Int. %** | **FHWM** | **Area** | **Phase** | **hkl** |
|---|---|---|---|---|---|---|
| 22.2899 | 3.98847 | 48.36 | 1.0558 | 89.55 | Bi | 003 |
| 27.0884 | 3.29185 | 75.23 | 0.2362 | 46.11 | Bi | 012 |
| 30.5675 | 2.92465 | 95.3 | 0.1771 | 43.8 | Sn | 200 |
| 31.9117 | 2.80446 | 100 | 0.2165 | 56.18 | Sn | 101 |
| 37.8999 | 2.374 | 31.41 | 0.1771 | 14.43 | Bi | 104 |
| 39.6036 | 2.27571 | 23.9 | 0.3149 | 19.53 | Bi | 110 |
| 43.7248 | 2.0703 | 40.49 | 0.1968 | 20.68 | Sn | 220 |
| 44.7451 | 2.02544 | 64.6 | 0.2952 | 49.48 | Bi | 110 |
| 45.79 | 1.98162 | 7.6 | 0.09 | 1.8 | Sn | 220 |
| 48.7147 | 1.86927 | 12.52 | 0.3149 | 10.23 | Bi | 110 |
| 55.1759 | 1.6647 | 10.57 | 0.3149 | 8.64 | Sn | 310 |
| 59.31 | 1.55815 | 2.28 | 0.09 | 0.54 | Bi | 107 |
| 61.17 | 1.51516 | 3.04 | 0.09 | 0.72 | Bi | 205 |
| 62.3849 | 1.48854 | 21.59 | 0.2362 | 13.23 | Bi | 107 |
| 64.4962 | 1.44482 | 19.87 | 0.3149 | 16.24 | Sn | 321 |
| 67.39 | 1.38965 | 2.28 | 0.09 | 0.54 | Bi | 018 |

**Table 1b**: x-ray analysis of $Sn_{76}Al_{10}Bi_9Cu_2Zn_2(TiO_2)_1$ alloy

| 2θ | d Å | Int. % | FHWM | Area | Phase | hkl |
|---|---|---|---|---|---|---|
| 70.81 | 1.33069 | 6.08 | 0.09 | 1.44 | Bi | 214 |
| 72.1809 | 1.30875 | 13.97 | 0.3149 | 11.41 | Sn | 420 |
| 75.47 | 1.25968 | 2.66 | 0.09 | 0.63 | Bi | 125 |
| 79.2736 | 1.20852 | 12.6 | 0.3936 | 12.87 | Sn | 312 |
| 85.11 | 1.13994 | 3.04 | 0.09 | 0.72 | Bi | 101 |
| 89.245 | 1.09752 | 6.08 | 0.4723 | 7.45 | Sn | 501 |
| 91.63 | 1.07509 | 2.28 | 0.09 | 0.54 | Bi | 312 |
| 95.3902 | 1.04154 | 4.66 | 0.576 | 9.42 | Sn | 332 |

**Table 1c**: x-ray analysis of $Sn_{76}Al_{10}Bi_{8.5}Cu_2Zn_2(TiO_2)_{1.5}$ alloy

| 2θ | d Å | Int. % | FHWM | Area | Phase | hkl |
|---|---|---|---|---|---|---|
| 22.5043 | 3.95094 | 12.09 | 0.5396 | 19.1 | Bi | 003 |
| 23.7276 | 3.74996 | 9.47 | 0.416 | 11.54 | Bi | 101 |
| 27.1586 | 3.2835 | 66.83 | 0.2165 | 62.68 | Bi | 012 |
| 30.5769 | 2.92378 | 82.99 | 0.2558 | 91.99 | Sn | 200 |
| 31.9844 | 2.79825 | 100 | 0.2558 | 110.84 | Sn | 101 |
| 37.9413 | 2.3715 | 31.4 | 0.2362 | 32.13 | Bi | 104 |
| 39.6171 | 2.27497 | 21.43 | 0.1968 | 18.27 | Bi | 110 |
| 43.7678 | 2.06837 | 47.66 | 0.2165 | 44.7 | Sn | 220 |
| 44.7907 | 2.02348 | 95.42 | 0.2165 | 89.5 | Bi | 110 |
| 45.9141 | 1.97655 | 5.39 | 0.3936 | 9.19 | Sn | 220 |
| 48.7094 | 1.86946 | 11.89 | 0.2755 | 14.2 | Bi | 110 |
| 55.1782 | 1.66463 | 14.74 | 0.3542 | 22.62 | Sn | 310 |
| 56.0704 | 1.64024 | 4.99 | 0.3149 | 6.81 | Bi | 107 |
| 59.3317 | 1.55764 | 2.81 | 0.4723 | 5.75 | Bi | 107 |
| 62.3739 | 1.48878 | 30.34 | 0.2165 | 28.46 | Bi | 107 |
| 63.654 | 1.46189 | 8.59 | 0.2755 | 10.26 | Bi | 107 |
| 64.4939 | 1.44487 | 30.66 | 0.2362 | 31.37 | Sn | 321 |
| 70.819 | 1.33054 | 5.89 | 0.2362 | 6.02 | Bi | 214 |
| 72.2188 | 1.30816 | 14.64 | 0.4723 | 29.96 | Sn | 420 |
| 72.9748 | 1.29646 | 13.01 | 0.1574 | 8.87 | Sn | 411 |
| 79.2891 | 1.20832 | 17.06 | 0.2165 | 16 | Sn | 312 |
| 89.1584 | 1.09837 | 8.49 | 0.3149 | 11.59 | Sn | 501 |
| 95.2935 | 1.04321 | 7.53 | 0.2362 | 7.7 | Sn | 332 |
| 97.3767 | 1.02552 | 3.45 | 0.768 | 15.53 | Sn | 521 |

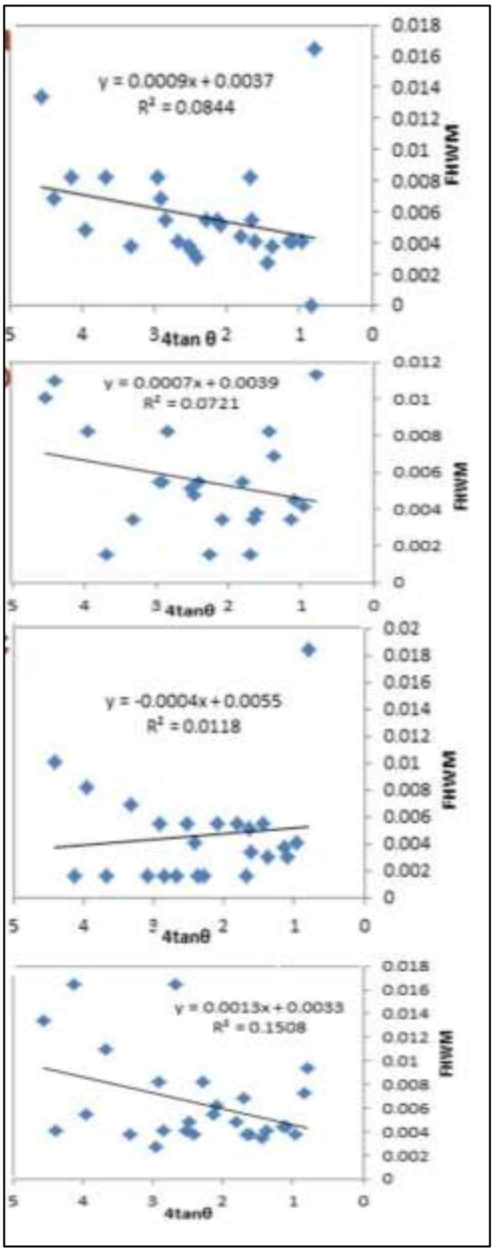


**Fig. 1e**: FHWM versus 4tanθ for $Sn_{76}Al_{10}Bi_{10-x}Cu_2Zn_2(TiO_2)_x$ alloys

***Scanning electron microscope analysis (SEM)***

Scanning electron micrographs of $Sn_{76}Al_{10}Bi_{10-x}Cu_2Zn_2(TiO_2)_x$ alloys are shown in Fig. 2. $Sn_{76}Al_{10}Bi_{10}Cu_2Zn_2$ has a large dendrite tin structure contained many small grains disturbed in it (white color), slabs from aluminum grain (bright white color) and large bismuth grain (black color). Adding different ratio from $TiO_2$ nanoparticles changed the shape and size of dendrite structure and disturbed dissolved atoms as grains in it. SEM analysis for used alloys shows heterogeneity structure and that is agreed with x-ray analysis.

***Internal friction and thermal diffusivity***

Internal friction measurements have been quick fruitful for learning about the behavior of metallic materials. Fig. 3 shows the resonance curves of $Sn_{76}Al_{10}Bi_{10-x}Cu_2Zn_2(TiO_2)_x$ alloys. Calculated internal friction and thermal diffusivity of $Sn_{76}Al_{10}Bi_{10-x}Cu_2Zn_2(TiO_2)_x$ alloys are listed in Table 2. Internal friction of $Sn_{76}Al_{10}Bi_{10}Cu_2Zn_2$ alloy decreased after adding titanium dioxide nanoparticles. Also thermal diffusivity increased (varied increased) up to 1 wt. % titanium dioxide and then decreased.

**Table 1d**: crystal size of β- Sn in $Sn_{76}Al_{10}Bi_{10-x}Cu_2Zn_2(TiO_2)_x$ alloys

| **Alloys** | **(Sn) τ ( Å)** |
|---|---|
| $Sn_{76}Al_{10}Bi_{10}Cu_2Zn_2$ | 347.647 |
| $Sn_{76}Al_{10}Bi_{9.5}Cu_2Zn_2(TiO_2)_{0.5}$ | 387.704 |
| $Sn_{76}Al_{10}Bi_9Cu_2Zn_2(TiO_2)_1$ | 383.817 |
| $Sn_{76}Al_{10}Bi_{8.5}Cu_2Zn_2(TiO_2)_{1.5}$ | 352.74 |

**Table 1e**: lattice microstrain of $Sn_{76}Al_{10}Bi_{10-x}Cu_2Zn_2(TiO_2)_x$ alloys

| **Alloys** | **(ε) x10$^{-3}$** |
|---|---|
| $Sn_{76}Al_{10}Bi_{10}Cu_2Zn_2$ | 0.9 |
| $Sn_{76}Al_{10}Bi_{9.5}Cu_2Zn_2(TiO_2)_{0.5}$ | 0.7 |
| $Sn_{76}Al_{10}Bi_9Cu_2Zn_2(TiO_2)_1$ | 0.4 |
| $Sn_{76}Al_{10}Bi_{8.5}Cu_2Zn_2(TiO_2)_{1.5}$ | 1.3 |

**Table 2**: internal friction and thermal diffusivity of $Sn_{76}Al_{10}Bi_{10-x}Cu_2Zn_2(TiO_2)_x$ alloys

| Alloys | $Q^{-1}$ | $D_{th}$ x $10^{-8}$ ($m^2$/sec) |
|---|---|---|
| $Sn_{76}Al_{10}Bi_{10}Cu_2Zn_2$ | 0.058 | 22.65 |
| $Sn_{76}Al_{10}Bi_{9.5}Cu_2Zn_2(TiO_2)_{0.5}$ | 0.0573 | 45.9 |
| $Sn_{76}Al_{10}Bi_9Cu_2Zn_2(TiO_2)_1$ | 0.0496 | 31.5 |
| $Sn_{76}Al_{10}Bi_{8.5}Cu_2Zn_2(TiO_2)_{1.5}$ | 0.0429 | 21.9 |

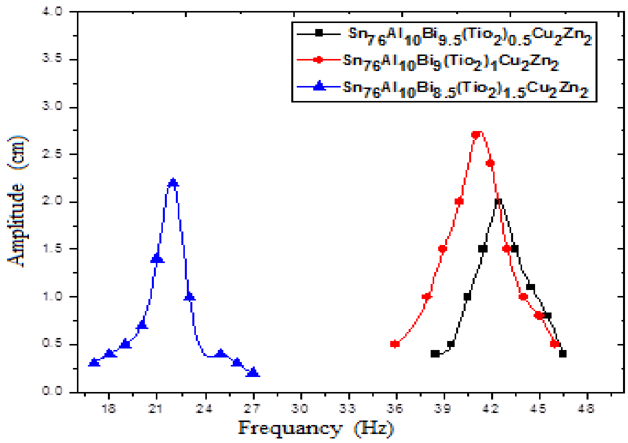


**Fig. 3**: resonance curves of $Sn_{76}Al_{10}Bi_{10-x}Cu_2Zn_2(TiO_2)_x$ alloys

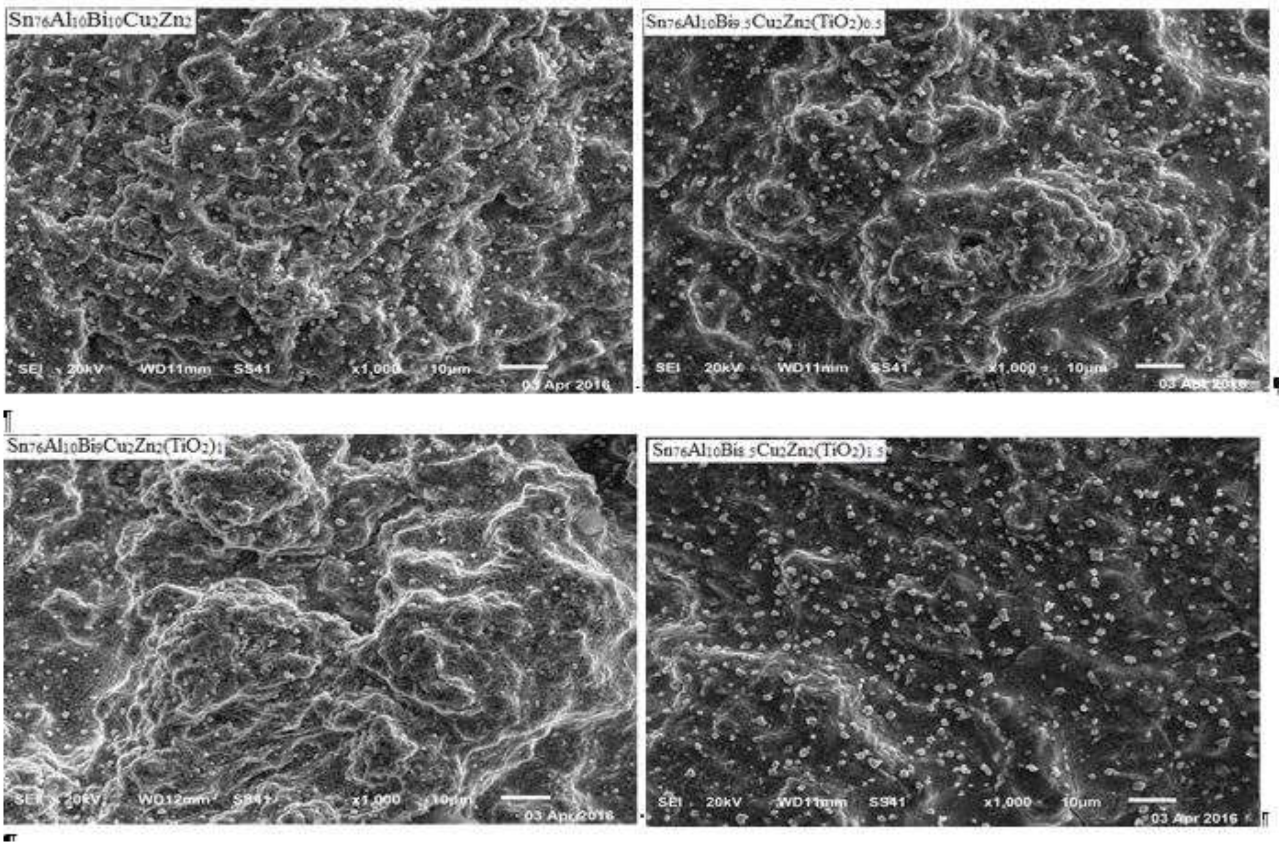


**Fig. 2**: SEM of $Sn_{76}Al_{10}Bi_{10-x}Cu_2Zn_2(TiO_2)_x$ alloys

***Vickers Microhardness and Maximum Shear Stress***

Vickers hardness of $Sn_{76}Al_{10}Bi_{10-x}Cu_2Zn_2(TiO_2)_x$ alloys at 10 gram force and indentation time 5 sec are presented in Table 3. Also the calculated maximum shear stress of used alloys is presented in Table 3. Vickers hardness value of $Sn_{76}Al_{10}Bi_{10}Cu_2Zn_2$ alloy decreased, (varied decreased), after adding titanium dioxide nanoparticles.

**Table 3**: Vickers hardness and maximum shear stress of used alloys

| lloys | $H_v$ kg/mm$^2$ | $\mu_n$ kg/mm$^2$ |
|---|---|---|
| $Sn_{76}Al_{10}Bi_{10}Cu_2Zn_2$ | 46.6±8.1 | 15.38 |
| $Sn_{76}Al_{10}Bi_{9.5}Cu_2Zn_2(TiO_2)_{0.5}$ | 24.4±1.4 | 8.05 |
| $Sn_{76}Al_{10}Bi_9Cu_2Zn_2(TiO_2)_1$ | 39.43±2.3 | 13.012 |
| $Sn_{76}Al_{10}Bi_{8.5}Cu_2Zn_2(TiO_2)_{1.5}$ | 42.2±4.2 | 13.93 |

***Electrochemical Corrosion Behavior***

Electrochemical polarization curves of $Sn_{76}Al_{10}Bi_{10-x}Cu_2Zn_2(TiO_2)_x$ alloys in 0.25 M HCl are shown in Fig. 4. The corrosion potential of $Sn_{76}Al_{10}Bi_{10-x}Cu_2Zn_2(TiO_2)_x$ alloys exhibited a negative potential. Also the cathodic and the anodic polarization curves exhibited similar corrosion trends. The corrosion current ($I_{Corr}$), corrosion potential ($E_{Corr}$) and corrosion rate (C. R) of $Sn_{76}Al_{10}Bi_{10-x}Cu_2Zn_2(TiO_2)_x$ alloys in 0.25 M HCl are presented in Table 4. Corrosion rate and corrosion current values of $Sn_{76}Al_{10}Bi_{10}Cu_2Zn_2$ alloy decreased after adding 0.5 and 1.5 wt. % titanium dioxide nanoparticles but they increased after adding 1 wt. %.

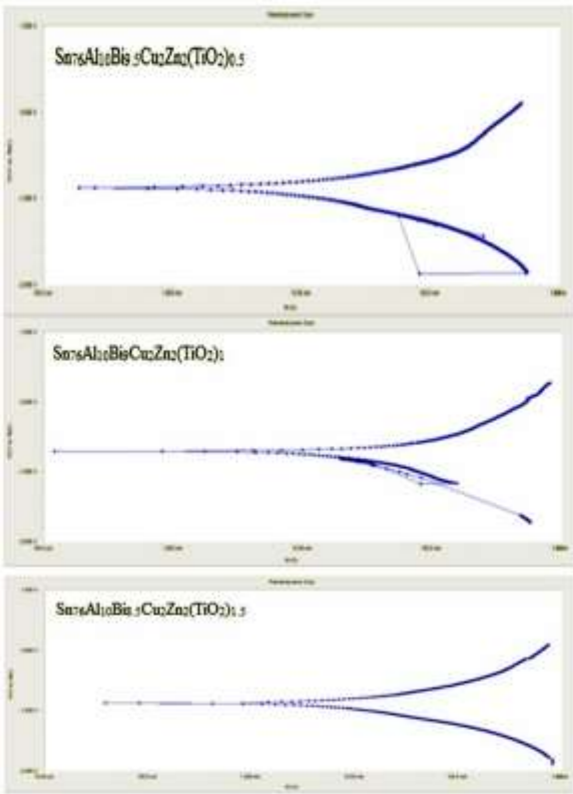


**Fig. 4**: electrochemical polarization curves of $Sn_{76}Al_{10}Bi_{10-x}Cu_2Zn_2(TiO_2)_x$ alloys

**Table 4**: $E_{corr}$, $I_{corr}$ and C. R of $Sn_{76}Al_{10}Bi_{10-x}Cu_2Zn_2(TiO_2)_x$ alloys

| Alloys | $E_{corr}$ mV | $I_{corr}$ μA | C. R mpy |
|---|---|---|---|
| $Sn_{76}Al_{10}Bi_{10}Cu_2Zn_2$ | -943 | 3.69 | 3.861e3 |
| $Sn_{76}Al_{10}Bi_{9.5}Cu_2Zn_2(TiO_2)_{0.5}$ | -873.0 | 3.27 | 3.424e3 |
| $Sn_{76}Al_{10}Bi_9Cu_2Zn_2(TiO_2)_1$ | -704.0 | 9.05 | 9.475e3 |
| $Sn_{76}Al_{10}Bi_{8.5}Cu_2Zn_2(TiO_2)_{1.5}$ | -875.0 | 2.92 | 3.085e3 |

The results of EFM experiments are a spectrum of current response as a function of frequency. Fig. 5 shows the intermodulation spectrum of $Sn_{76}Al_{10}Bi_{10-x}Cu_2Zn_2(TiO_2)_x$ alloys s in 0. 25 M HCl solutions. The larger peaks were used to calculate the corrosion current density and the corrosion rate whish presented in Table 5. Corrosion rate value of $Sn_{76}Al_{10}Bi_{10}Cu_2Zn_2$ alloy decreased, varied decreased, after adding titanium dioxide nanoparticles but corrosion current density increased, varied increased, after adding titanium dioxide nanoparticles.

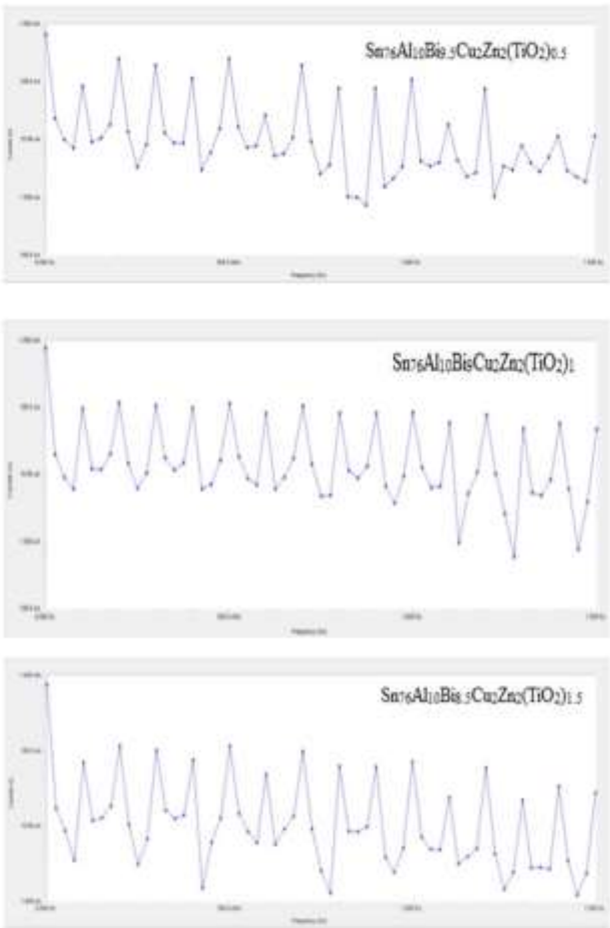

**Fig. 5**: The intermodulation spectrum of $Sn_{76}Al_{10}Bi_{10-x}Cu_2Zn_2(TiO_2)_x$ alloys

**Table 5**: $i_{corr}$ and C. R of $Sn_{76}Al_{10}Bi_{10-x}Cu_2Zn_2(TiO_2)_x$ alloys

| Alloys | $i_{corr}$ μA | C. R mpy |
|---|---|---|
| $Sn_{76}Al_{10}Bi_{10}Cu_2Zn_2$ | 29.92 | 31.33e3 |
| $Sn_{76}Al_{10}Bi_{9.5}Cu_2Zn_2(TiO_2)_{0.5}$ | 161.6 | 169.3 |
| $Sn_{76}Al_{10}Bi_9Cu_2Zn_2(TiO_2)_1$ | 62.44 | 65.38 |
| $Sn_{76}Al_{10}Bi_{8.5}Cu_2Zn_2(TiO_2)_{1.5}$ | 66.74 | 69.89 |

***Thermal Behaviour and Parameters***

Thermal analysis is used to study solid state transformations as well as solid liquid reactions. They depend on the nature of solid phase and on its temperature. The DSC thermographs were obtained with heating rate 10 °C /min in the temperature range 0- 400 °C. Fig. 6 shows the DSC thermographs of $Sn_{76}Al_{10}Bi_{10-x}Cu_2Zn_2(TiO_2)_x$ alloys**.** No significant effect on melting temperature value of $Sn_{76}Al_{10}Bi_{10}Cu_2Zn_2$ alloy after adding titanium dioxide nanoparticles as presented in Table 6.

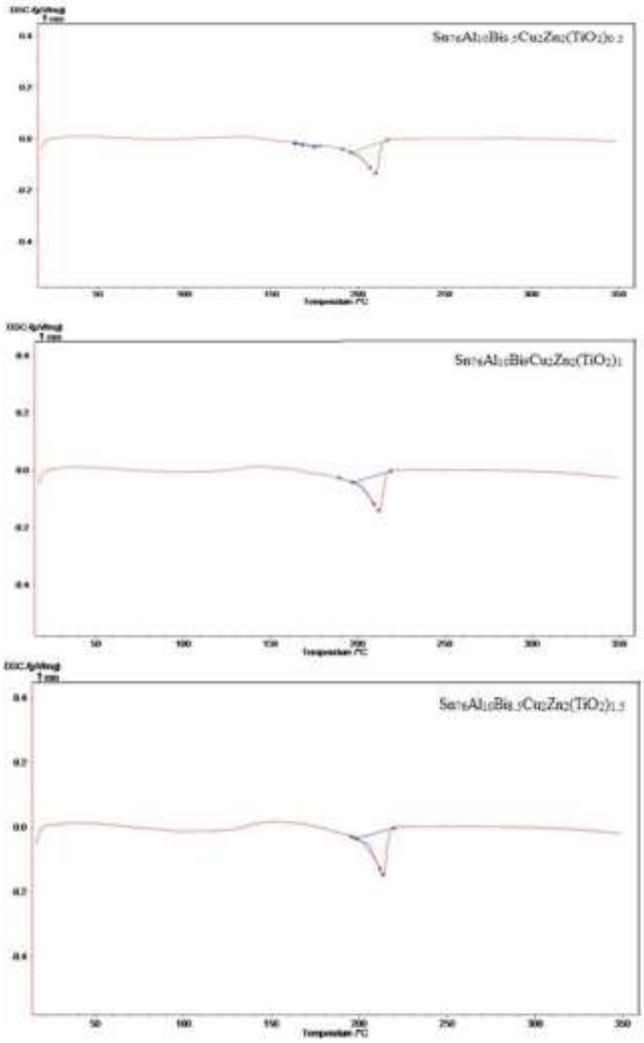

**Fig. 6**: DSC graphs of used alloys

**Table 6**: Melting temperature of used alloys

| Alloys | Melting temperature °C |
|---|---|
| Sn76Al10Bi10Cu2Zn2 | 212 |
| Sn76Al10Bi9.5Cu2Zn2(TiO2)0.5 | 210.1 |
| Sn76Al10Bi9Cu2Zn2(TiO2)1 | 212.3 |
| Sn76Al10Bi8.5Cu2Zn2(TiO2)1.5 | 213.8 |

## Conclusion

Lattice microstrain of $Sn_{76}Al_{10}Bi_{10}Cu_2Zn_2$ alloy decreased after adding titanium dioxide up to 1 wt. % and then increased. Internal friction of $Sn_{76}Al_{10}Bi_{10}Cu_2Zn_2$ alloy decreased after adding titanium dioxide nanoparticles. Corrosion rate and corrosion current values of $Sn_{76}Al_{10}Bi_{10}Cu_2Zn_2$ alloy decreased after adding 0.5 and 1.5 wt. % titanium dioxide nanoparticles but they increased after adding 1 wt. %. Corrosion rate value of $Sn_{76}Al_{10}Bi_{10}Cu_2Zn_2$ alloy decreased, varied decreased, after adding titanium dioxide nanoparticles but corrosion current density increased, varied increased, after adding titanium dioxide nanoparticles. No significant effect on melting temperature value of $Sn_{76}Al_{10}Bi_{10}Cu_2Zn_2$ alloy after adding titanium dioxide nanoparticles

## References


Berry BS and Pritchett WC (1973) Some physical properties of two amorphous metallic alloys. *Journal of Applied Physics* **44**: 3122- 3126. DOI: 10.1063/1.1662718

Cullity BD (1959) *Element of x-ray diffraction*, Ch.10: 297

Desaki T, Goto Y and Kamiya S (2000) Development of the aluminum alloy bearing with higher wear resistance. *JSAE Review* **21**: 321-325. DOI: 10.1016/S0389-4304(00)00051-5

El-Bediwi A, Lashin AR, Mossa M, Kamal M (2011) Indentation creep and mechanical properties of quaternary Sn-Sb based alloys. *Material Science and Engineering* A528: 3568. DOI: 10.1016/j.msea.2011.01.054

El-Bediwi AB (2004) Effects of Cu and Ag as ternary and quaternary additions on some physical properties of SnSb7 bearing alloy. *Radiation Effects & Defects in Solids* **159**: 125- 132. DOI: 10.1080/10420150310001654052

El-Bediwi AB (2004) Effects of heat treatment and additions on dynamic mechanical properties of quenched SnSb bearing alloy. *Radiation Effects & Defects in Solids* **159**: 539-542. DOI: 10.1080/10420150412331326903

El-Bediwi AB, Al-Bawee A and Kamal M (2015) Corrosion behavior and physical properties ofmodified tin- antimony bearing alloy. *Materials Science: An Indian Journal* **13**(4): 136.

El-Bediwi AB, Al-Bawee A and Kamal M (2015) Effect of Titanium Oxide on Structure, Bearing Properties of Tin-Antimony-Lead and Tin-Aluminum Alloys. *International Journal of Science and Engineering Applications* **4**(2): 46-53. DOI: 10.7753/IJSEA0402.1005

El-Bediwi AB, El-Shafei A, Kamal M (2015) Effect of alloying elements on structure, physical and chemical properties of SnBiZn solder alloy. *Materials Science: An Indian Journal* **13**(1): 1-13.

El-Bediwi AB, Grayb M and Kamal M (2015) Influence of Titanium Oxide on Creep Behavior, Microstructure and Physical Properties of Tin-Antimony and Tin-Aluminum-Antimony Based Bearing Alloys. *International Journal of Science and Engineering Applications* **4**(2): 64-70. DOI: 10.7753/IJSEA0402.1008

Esfandyarpour M.J, Mahmudi R (2011) Microstructure and tensile behavior of Sn-5Sb lead-free solder alloy containing Bi and Cu. Material Science and Engineering A 530: 402-410. DOI: 10.1016/j.msea.2011.09.103

Forrester PG (1960) *Metallic Review* **5**: 507. DOI: 10.1179/mtlr.1960.5.1.507

Forrester PG (1961) *Curr. Eng. Pract*. **3**: 4.

Kamal M, El-Bediwi A and El-Shobaki MR (2006) Influence of alloying elements on structure and some physical properties of quenched Sn- Sb alloy. *Radiation Effects& Defects in Solids* **161**: 549-557. DOI: 10.1080/10420150600825925

Lepper K, James M, Chashechkina J and Rigney DA (1997) Sliding behavior of selected aluminum alloys. *Wear* **203**: 46-56.

Pathak JP and Mohan S (2003) Tribological Behavior of Conventional Al-Sn and Equivalent Al-Pb Alloys under Lubrication. *Bulletin Material Science* **26**(3): 315. DOI: 10.1007/BF02707453

Pratt GC (1973) *International Metallic Review* **18**: 62. DOI: 10.1179/imr.1973.18.2.62

Schreiber E, Anderson OL and Soga N (1973) *Elastic Constants and their Measurement*, McGraw-Hill Book Company Ch. 4

Tegart WIM (1966) *Elements of mechanical metallurgy*. New York: The MacMillan Co., 91

Timoshenko S and Goddier JN (1951) *Theory of elasticity*, 2nd Ed", McGraw-Hill, New York 277